

## General Disclaimer

### One or more of the Following Statements may affect this Document

- This document has been reproduced from the best copy furnished by the organizational source. It is being released in the interest of making available as much information as possible.
- This document may contain data, which exceeds the sheet parameters. It was furnished in this condition by the organizational source and is the best copy available.
- This document may contain tone-on-tone or color graphs, charts and/or pictures, which have been reproduced in black and white.
- This document is paginated as submitted by the original source.
- Portions of this document are not fully legible due to the historical nature of some of the material. However, it is the best reproduction available from the original submission.

R-917

**FINAL REPORT  
TEST EVALUATION OF THE SPERRY LASER GYRO  
MODEL ASLG 15**

by

**Stephen Helfant**

**September 1975**

(NASA-CF-144227) TEST EVALUATION OF THE  
SPERRY LASER GYRO MODEL ASLG 15 Final  
Report (Draper (Charles Stark) Lab., Inc.)  
38 p HC \$4.00 CSCI 14P

N76-22511

Unclas  
G3/35 25275



**The Charles Stark Draper Laboratory, Inc.**

Cambridge, Massachusetts 02139



**Distribution limited to US Government agencies only. (Test and Evaluation) September 1975. Other requests for this document must be referred to NASA/MSFC.**




R-917

FINAL REPORT  
TEST EVALUATION OF THE SPERRY LASER GYRO  
MODEL ASLG 15

by

Stephen Helfant

September 1975

Approved: 

Date 

N. Sears

THE CHARLES STARK DRAPER LABORATORY, INC.  
CAMBRIDGE, MASSACHUSETTS  
02139

## ACKNOWLEDGEMENT

This report was prepared by The Charles Stark Draper Laboratory, Inc. under Contract NAS8-30255 for the George C. Marshall Space Flight Center of the National Aeronautics and Space Administration.\*

The author wishes to acknowledge the contributions made to this report by Jerold Gilmore, Division Director, and Julius Feldman, Program Manager. Mr. Gilmore and Mr. Feldman helped in the review and many of their suggestions have been included. The contributions made by John Sinkiewicz, the initial Program Manager, are also acknowledged.

Appreciation is extended to Bobby Walls, Technical Monitor, for his years of dedicated effort in laser gyro evaluation and design improvement which have made the laser gyro a reliable strapdown inertial sensor. His requirement for an independent laser gyro evaluation made this test effort possible.

The assistance afforded by Warren Macek of the Sperry Rand Corporation is greatly appreciated.

This volume is the combined effort of the following additional people:

Ron Rabitz and Martin Landey for editorial suggestions.

Dale Woodbury, Ernie Portway and Ed Ryan for technical assistance in the laboratory.

Linda Willy for her work on the illustrations presented in this report.

Jean Pennick for technical typing.

The publication of this report does not constitute approval by the National Aeronautics and Space Administration of the findings or the conclusions contained herein. It is published only for the exchange and stimulation of ideas.

\* This effort is being continued under Contract NAS1-13958 for the NASA/Langley Research Center.

## ABSTRACT

This report presents a test evaluation of the Sperry laser gyro model ASLG 15. The bias, scale factor, scale factor sensitivity to supply voltage and external temperature, and turn-on trends are evaluated.

## TABLE OF CONTENTS

<u>Section</u>		<u>Page</u>
1	INTRODUCTION AND SUMMARY.....	1-1
	1.1 Introduction.....	1-1
	1.2 Summary .....	1-1
2	TERMINOLOGY .....	2-1
3	LASER GYRO CONCEPT.....	3-1
4	SYSTEM DESCRIPTION AND PERFORMANCE CHARACTERISTICS .....	4-1
	4.1 Physical Description.....	4-1
	4.2 Electronics Description .....	4-1
	4.3 Operational Requirements and Performance Specifications .....	4-5
5	TEST EQUIPMENT AND PROCEDURES.....	5-1
	5.1 Test Equipment.....	5-1
	5.2 Test Procedures.....	5-1
6	TEST RESULTS	
	6.1 Bias Test Results.....	6-1
	6.2 Scale Factor Test Results .....	6-6
7	RECOMMENDATIONS.....	7-1

PRECEDING PAGE BLANK NOT FILMED

## LIST OF ILLUSTRATIONS

<u>Figure</u>		<u>Page</u>
3-1	Laser gyro-optical schematic.....	3-1
4-1	Sperry model ASLG 15 laser gyro.....	4-2
4-2	Sperry laser gyro-optical schematic.....	4-2
4-3	Functional block diagram.....	4-4
5-1	Test facility at The Charles Stark Draper Laboratory .....	5-2
6-1	Bias stability (4-03-75) .....	6-2
6-2	Bias stability (4-11-75) .....	6-3
6-3	Drift repeatability across turn-offs and cooldowns .....	6-6
6-4	Scale factor: initial transient after warm-up ( $10^{\circ}/s$ , cw).....	6-7
6-5	Scale factor: initial transient after warm-up ( $30^{\circ}/s$ , cw).....	6-7
6-6	Scale factor: initial transient after warm-up ( $70^{\circ}/s$ , cw).....	6-8
6-7	Scale factor: initial transient after warm-up (same rate from day to day).....	6-8
6-8	Scale factor decay after initial transient (four different rates).....	6-9
6-9	Scale factor decay after initial transient (same rate from day to day).....	6-10
6-10	Long-term scale factor stability.....	6-11
6-11	Scale factor variation with rate ( $5^{\circ}/s$ to $100^{\circ}/s$ ) .....	6-12
6-12	Scale factor variation with rate ( $1^{\circ}/s$ to $12^{\circ}/s$ ) .....	6-13
6-13	Scale factor vs. calendar time.....	6-14



## LIST OF TABLES

<u>Table</u>		<u>Page</u>
1-I	Sperry laser gyro performance characteristics (CSDL data).....	1-2
4-I	Operational environment (Sperry data).....	4-6
4-II	Performance characteristics (Sperry data).....	4-6
6-I	Bias stability and random drift.....	6-4

## SECTION 1

### INTRODUCTION AND SUMMARY

#### 1.1 INTRODUCTION

This is the final report of the ring laser gyro (RLG) evaluation section of NASA/MSFC contract number NAS8-30255. The work statement was as follows:

"Test the laser gyro in accordance with the following test plan.

- (1) Fabricate and integrate holding fixtures, adapter, computer interface and special test equipment required to perform the test program.
- (2) Perform integrated tests to verify the proper operation of the assembled test set up.
- (3) Perform a fixed azimuth, drift stability test.
- (4) Perform single axis, constant rate tests with clockwise and counter-clockwise rates at intervals from 5 to 100 degrees per second.
- (5) Reduce data and evaluate test results for inclusion in the final report."

In addition to reporting the tasks specified in the contract statement of work, this report contains test results on the long-term bias and scale factor (SF) repeatability, illustrates the transient and decay characteristics of the SF after instrument turn-on, presents results of low rate input investigations ( $1^{\circ}/s$  to  $12^{\circ}/s$ ) and quantitatively shows the SF sensitivity to voltage and mounting plate temperature changes.

Testing started on 5 March 1975 and ended on 11 July 1975. No adjustments were made to the instrument, which was tested as configured upon arrival from NASA/MFSC, during this test period.

The laser gyro tested was a model ASLG-15, serial number 3B, manufactured by the Sperry Gyroscope Company in October 1973.

#### 1.2 SUMMARY

The results of the test evaluation on the Sperry laser gyro are summarized in Table 1-1. The information in this table was derived from the findings contained in Section 6, "Test Results".

Table 1-1. Sperry laser gyro performance characteristics (CSDL data)

I. Warm-up (instrument constraint - no meaningful output)	20-25 min.
II. Bias	
A. Initial Transient (after warm-up)	
(1) Duration	0.5 h
(2) Amplitude	1°/h
B. Decay Characteristics (after warm-up and transient)	None
C. Magnitude (after warm-up and transient) Note: Magnitude plus $\omega_{IEV} = 3.8^\circ/h$	-6.3°/h
D. Variation of Sigma with Sampling Time (s)	
$\Delta T = 60$	} White Noise Characteristic $\frac{\sigma_1}{\sigma_2} = \sqrt{\frac{\Delta T_2}{\Delta T_1}}$
$\Delta T = 100$	
$\Delta T = 600$	
$\Delta T = 3600$	
0.23°/h	
0.16°/h	
0.07°/h	
0.03°/h	
E. Long-Term Repeatability (45 days) - 1 Sigma	
(1) One Hour of data, one hour after turn-on	0.04°/h
(2) One 100 s sample, immediately after warm-up	0.2°/h
Note: Each test was performed after an overnight turn-off	
III. Scale Factor	
A. Initial Transient	
(1) Duration	0.5 h
(2) Amplitude (max.)	
a. 10°/s	280 ppm
b. 30°/s	240 ppm
c. 70°/s	70 ppm
B. Decay Characteristics (after warm-up and transient)	
(1) Time Constant	>4 h
(2) Amplitude (first 8 hours)	
a. 10°/s	220 ppm
b. 30°/s	120 ppm
c. 70°/s	90 ppm
C. Stability (peak-to-peak 36 hours after warm-up at 70°/s, cw)	8 ppm
D. Linearity - One Sigma	
(1) 5°/s to 100°/s	100 ppm
(2) 1°/s to 12°/s	90 ppm
E. Long Term Drift - Amplitude (90 days across turn-offs)	
(1) 10°/s	420 ppm
(2) 20°/s	630 ppm
(3) 70°/s } Primarily due to a drift in fixed bias of =40°/h	130 ppm
F. SF Sensitivities	
(1) Supply Voltage (28±2 Vdc)	None
(2) Mounting Plate Temperature (90±2°F)	3 ppm/°F

## SECTION 2

### TERMINOLOGY

This section defines the RLG terms used in this report.

Bias:

Average output after inertial angular rate inputs are removed (expressed in degrees per hour).

Bias Stability:

The one-sigma value of the RLG bias after initial transients. (See "random drift" for noise in the RLG bias as a function of the sampling period.)

Decay:

The settling characteristic after any initial transients.

Input Axis (IA):

Axis perpendicular to the plane of the laser beam path.

Input Rate

Angular displacement of the case about the input axis per unit time.

Lock-In:

At low input rates the frequencies of the two counter-rotating beams are very close to each other. Because of optical scattering, the two beams lock together (lock-in) and no output is obtained in the presence of real inputs. This phenomenon is circumvented by an anti-lock-in mechanism and/or a compensation technique.

Random Drift:

Measure of the noise in the RLG bias. It is determined as a function of the sampling period from the one-sigma bias stability value. For the Sperry ring laser gyro the random drift is proportional to the reciprocal of the square root of the sampling period (a characteristic of white noise).

Sampling Period:

Time allowed for the RLG net output count to accumulate in the counter before resetting.

Scale Factor:

The ratio that relates the inertial-frame rotations about the gyro input axis to the gyro output (expressed in arc sec/pulse).

Scale Factor Linearity:

The standard deviation of the average scale factor at various constant rates of rotation covering the dynamic range of the RLG (the contract required  $5^{\circ}/s$  to  $100^{\circ}/s$ ). If the slope is compensable, the best fit curve may be used to calculate the standard deviation (expressed in parts per million).

Scale Factor Stability:

Peak-to-peak spread and/or standard deviation in data during a selected test interval for a constant input rate (expressed in parts per million).

Turn-On Trends:

Changes in the RLG bias or scale factor that occur for a short period after the instrument starts to operate.

### SECTION 3

#### RING LASER GYRO CONCEPT

This section presents an elementary discussion of the Sperry ring laser gyro concept and is included in this report for the reader who is unfamiliar with laser gyros. The conventional ring laser gyro has two laser beams traveling along the same closed path in opposite directions. Figure 3-1 is an optical schematic diagram. Any rotation about the axis perpendicular to the plane of the light path, defined as the input axis (IA), is sensed as a change in path length. If the rotation is clockwise the clockwise beam travels a longer distance around the light path, while the counter-clockwise laser beam travels a shorter distance.

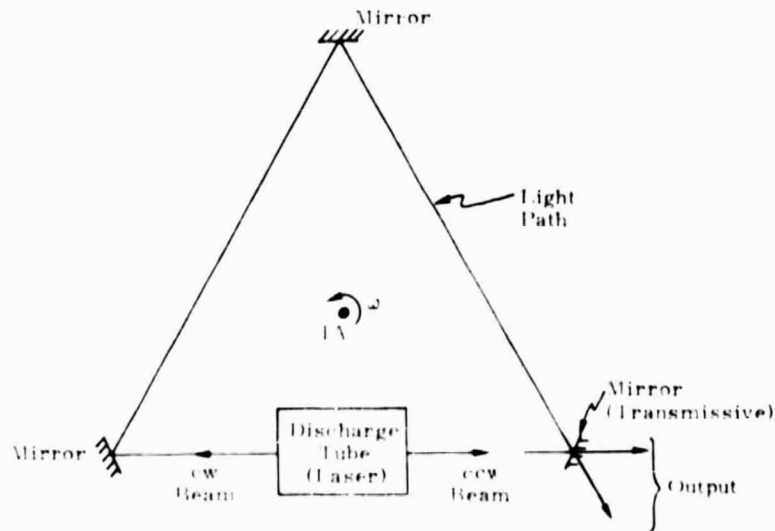


Figure 3-1. Laser gyro-optical schematic.

The operational requirements for the instrument are:

- (1) The conditions for lasing (such as gain, beam loss, path length equal to an integral number of wavelengths, etc.) must be satisfied, and
- (2) A biasing technique must be used to avoid lock-in problems.

The output of the laser gyro depends primarily on the change in frequency of each laser beam during rotation. The basic ideal equation shows the relationship of the output frequency shift,  $\Delta f$ , to the input rate as follows:

$$\Delta f = \frac{4\mathbf{A} \cdot \boldsymbol{\omega}}{\lambda L} + \Omega_B$$

where:

$\mathbf{A}$  = vector representing and normal to the area enclosed by the light path.

$\boldsymbol{\omega}$  = input rate vector.

$\Omega_B$  = biasing effect frequency.

$\lambda$  = wave length of the laser beam.

$L$  = path length.

Samples of the two beams are brought together through an output mirror and combining prism. The phase shift between the two beams is determined using photo-electric detectors, and the beat frequency output is the measure of rotation rate. The scale factor relating output frequency to input angular velocity is a function of the size and shape of the ring. Pulse shaping circuits are used to convert the sinusoidal output to pulses of the desired form.

One of the design problems of the laser gyro is lock-in. At low input rates the unbiased frequencies of the two counter-rotating beams are very close to each other. Because of optical scattering, the two beams lock together (lock-in) and no output is obtained. This problem has been circumvented by a variety of techniques which produce an effective frequency difference between the two beams and prevent the instrument from synchronizing to a single frequency in the lock-in region.

The biasing technique in the ASLG-15 laser gyro uses a magnetic mirror designed to optically create a gyro output.

## SECTION 4

### SYSTEM DESCRIPTION AND PERFORMANCE CHARACTERISTICS

This section describes the physical dimensions, electronics components, operational requirements and performance characteristics of the Sperry single-axis strapdown laser gyro system, model ASLG 15. The information was obtained from the "Sperry Installation, Operation and Performance Manual,- November 20, 1974".

#### 4.1 PHYSICAL DESCRIPTION

The Sperry laser gyro system consists of two assemblies, the sensor and the control electronics/power supply (EA). The pie shape sensor assembly is shown in Fig. 4-1. It measures 8 inches across the base with a height of 5 inches and a thickness of 2.5 inches. The optical cavity forms a triangular light path 5 inches on a side. The primary structure is made of aluminum and the biasing element is a magnetic mirror. The entire structure, surrounded by a three layer magnetic shield, is evacuated and sealed. The control electronics/power supply assembly is packaged separately from the sensor and measures approximately 8 x 7 x 5 inches.

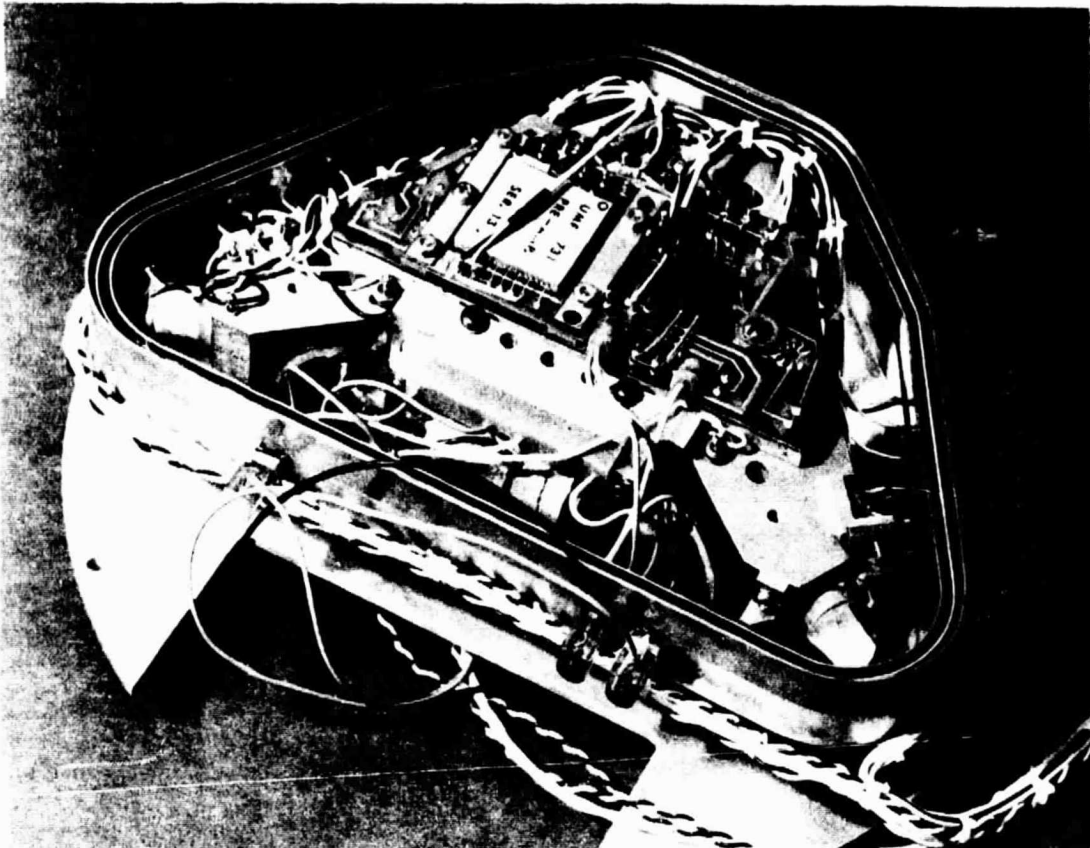
Figure 4-2 is an optical schematic illustrating the major components.

The ASLG-15 gyro requires a thermally controlled base mount to decrease warm-up time and lessen heat losses to the environment. In addition to the preheated base mount, thermal insulation around the instrument is also suggested by the manufacturer to minimize thermal gradients. In compliance with these requirements, the sensor was tested with a preheated base mount and an insulated shroud.

#### 4.2 ELECTRONICS DESCRIPTION

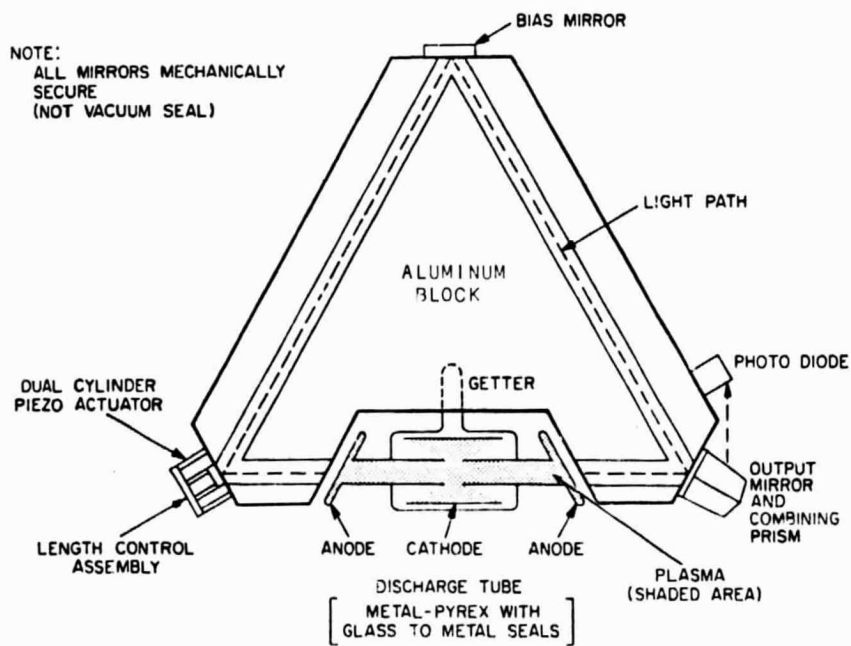
The gyro output, a sinusoidally varying electrical signal whose frequency is proportional to body input rate plus the optically applied bias, is fed to a rate preprocessor in the control electronics assembly. The output of the control electronics consists of two serial pulse lines representing angle increment and direction of rotation.





(Courtesy of Sperry Gyroscope)

Figure 4-1. Sperry model ASLG 15 laser gyro.



(Courtesy of Sperry Gyroscope)

Figure 4-2. Sperry laser gyro-optical schematic.

This single axis system contains all the control circuits necessary for laser gyro operation. The following two sections describe the laser gyro control and the signal conditioner electronics.

#### 4.2.1 Laser Gyro Control Electronics

Figure 4-3 is a simplified functional block diagram of the system electronics. Two of the three required laser gyro control circuits are packaged within the sensor assembly. This circuitry, magnetic mirror bias control and discharge current regulation, are in two hybrid packages mounted directly to the aluminum sensor cavity structure. They have been included in the sensor to take advantage of the thermally controlled environment.

The bias control electronics provides magnetic mirror current regulations and control for the gyro. It contains the switching circuits that respond to input signals that control the polarity of the applied bias. These polarity control signals are square waves having a 2 second period that alternate the applied optical bias as described below.

Two forms of discharge tube current regulation are provided, differential current control and total current control. The laser gyro discharge tube is a double anode, single cathode device. The two anodes are provided to split the discharge, thereby minimizing the Langmuir flow in the gas discharge. (Residual Langmuir flow creates an inherent instrument bias.) Changes in flow, therefore, are directly related to changes in gyro drift. Differential current control is incorporated to minimize this source of gyro drift.

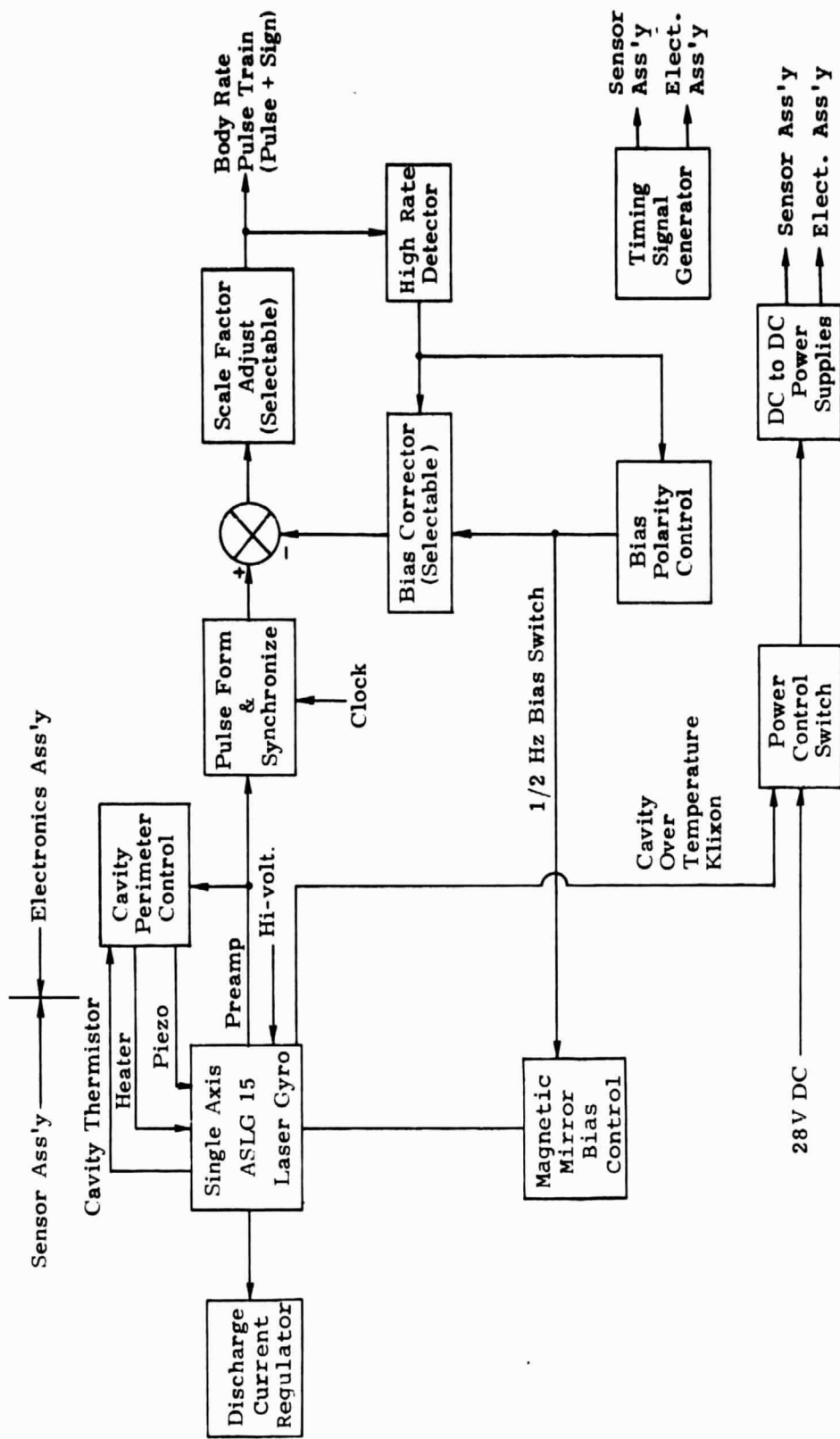
The total discharge current is controlled to maintain the laser gyro gain-to-loss ratio, thereby stabilizing its performance characteristic.

The remaining laser gyro control electronics functions, performed in the electronics assembly, consist of the following.

- Closed loop sensor assembly temperature control.
- Closed loop cavity length control.

The temperature loop controls the laser gyro optical cavity temperature. During the warm-up cycle, the heater loop operates in response to a cavity mounted thermistor bridge signal. Upon completion of warm-up (cavity at approximately 130 °F), the heater loop is switched to cavity perimeter servo control.

The cavity perimeter length control loop provides short term control through piezoelectric actuator response. Long term adjustment is accomplished through the cavity heater.



(Courtesy of Sperry Gyroscope)

Figure 4-3. Functional block diagram.

#### 4.2.2 Signal Conditioner Electronics

The signal conditioner operates on the sinusoidal laser gyro output signal to provide a measure of sensor assembly rotation angle. The following functions are provided.

The processor uses DDA techniques to derive the desired output. A timing signal generator develops all timing signals and clock pulses required for this operation.

A pulse former converts the laser sine wave into a pulse train having the same frequency as the original signal. A synchronizer stores the pulses for strobing by the processor timing.

The bias polarity control commands of the magnetic mirror coil current to reverse polarity at one second intervals, and selects the bias compensation required for the instantaneous bias polarity.

A high rate level detector senses rate in excess of  $12.5^{\circ}/\text{sec}$  and switches to fixed bias to prevent the rotation from causing a lock-in condition and to avoid ambiguity in rotation direction and rate output.

The bias corrector removes bias pulses from the incoming signal so that the remaining pulse rate is proportional to sensor input rate. The actual correction rate is selectable.

The scale factor of the net pulse train can be adjusted from the 3.3 arc sec/pulse to any desired output pulse weight (greater than 3.3 arc sec/pulse) with 16 bit accuracy. The scale factor is selectable via a plug board.

The computed angle (increment) available in pulse form:

- Logic "0" is  $.5 \pm .5$  Vdc.
- Logic "1" is  $4.5 \pm .5$  Vdc.
- Pulse resolution minimum is 3.3 arc sec/pulse

#### 4.3 OPERATIONAL REQUIREMENTS AND PERFORMANCE CHARACTERISTICS

The laser gyro system operates on 28 Vdc. It consumes approximately 100 watts for turn-on and warm-up, and 40 watts for steady state operation.

With the power applied the system can be made operative by moving the power toggle switch, located on the front panel to the ON position. This initiates an automatic warm-up procedure that brings the sensor and mounting base thermistors to within a few degrees of the normal operating temperature. When the unit is ready for operation, the READY light on the front panel is lit. CSDL data shows that the instrument requires 20 to 25 minutes to warm-up after excitation of the laser's electronic assembly.

The operating environment defined by Sperry is summarized in Table 4-I.

Nominal performance characteristics quoted by Sperry for their aluminum instruments with a magnetic mirror are summarized in Table 4-II.

Table 4-I. Operational environment (Sperry data)

<u>Input Dynamics</u>	Sperry
Angular Rate Range	$\pm 110^\circ/\text{s}$
Angular Acceleration Range	$\pm 1000^\circ/\text{s}^2$
Linear Acceleration	10 g
<u>Temperature Range</u>	0 to $100^\circ\text{F}$

Table 4-II. Performance characteristics\* (Sperry data)

	Sperry (Population)
<u>Bias</u>	
Random Drift ( $1\sigma$ )	$.03^\circ/\text{h}/\sqrt{\text{h}}$
30-Day Turn-on Repeatability ( $1\sigma$ )	$0.2^\circ/\text{h}$
<u>Scale Factor</u>	
Nominal Value (Selectable)	$3.3 \widehat{\text{sec}}/\text{p}$
Linearity Error ( $\pm 100^\circ/\text{s}$ input)	$\pm 100$ ppm
30-Day Turn-on Repeatability	$\pm 200$ ppm

\* The number of cooldowns and the duration of warm-up before each test were not defined by Sperry.

## SECTION 5

### TEST EQUIPMENT AND PROCEDURES

#### 5.1 TEST EQUIPMENT

The six pieces of equipment used in testing the RLG and their functions are:

- (1) Air Bearing Test Table - Goerz model 500-581 used to provide a static base for drift tests and precise rotation rates for scale factor tests.
- (2) Reversible Counter - IRA model 601 used to count RLG output and transfer a print command without loss of data.
- (3) Printer - Beckman model 1453A used to print the net RLG output count (accurate to plus or minus one pulse).
- (4) Punch - Invac Corp. model 10135 used in conjunction with the printer to obtain a paper tape for computer-aided evaluation.
- (5) Power Supply - Perkin model TVR 040-20-15 which supplied 28 volts dc at 3A to the RLG and test equipment.
- (6) Temperature Controller - used to maintain the temperature of the base mount at  $90 \pm 1^{\circ}\text{F}$ .

Figure 5-1 is a photograph of the test facility used to evaluate the laser gyro at the C. S Draper Lab., Inc.

#### 5.2 TEST PROCEDURES

##### 5.2.1 Instrument Bias

The test table is locked into position and the net count of the RLG output is measured for various sampling times. To calculate the absolute magnitude of the bias the IA misalignment has to be measured accurately to determine earth rate input. For this testing, the absolute magnitude of the bias was not required and the table was locked into one consistent orientation. The majority of the bias tests used a 100 second sampling period and a test duration of one hour;

REPRODUCIBILITY OF THE ORIGINAL PAGE IS POOR

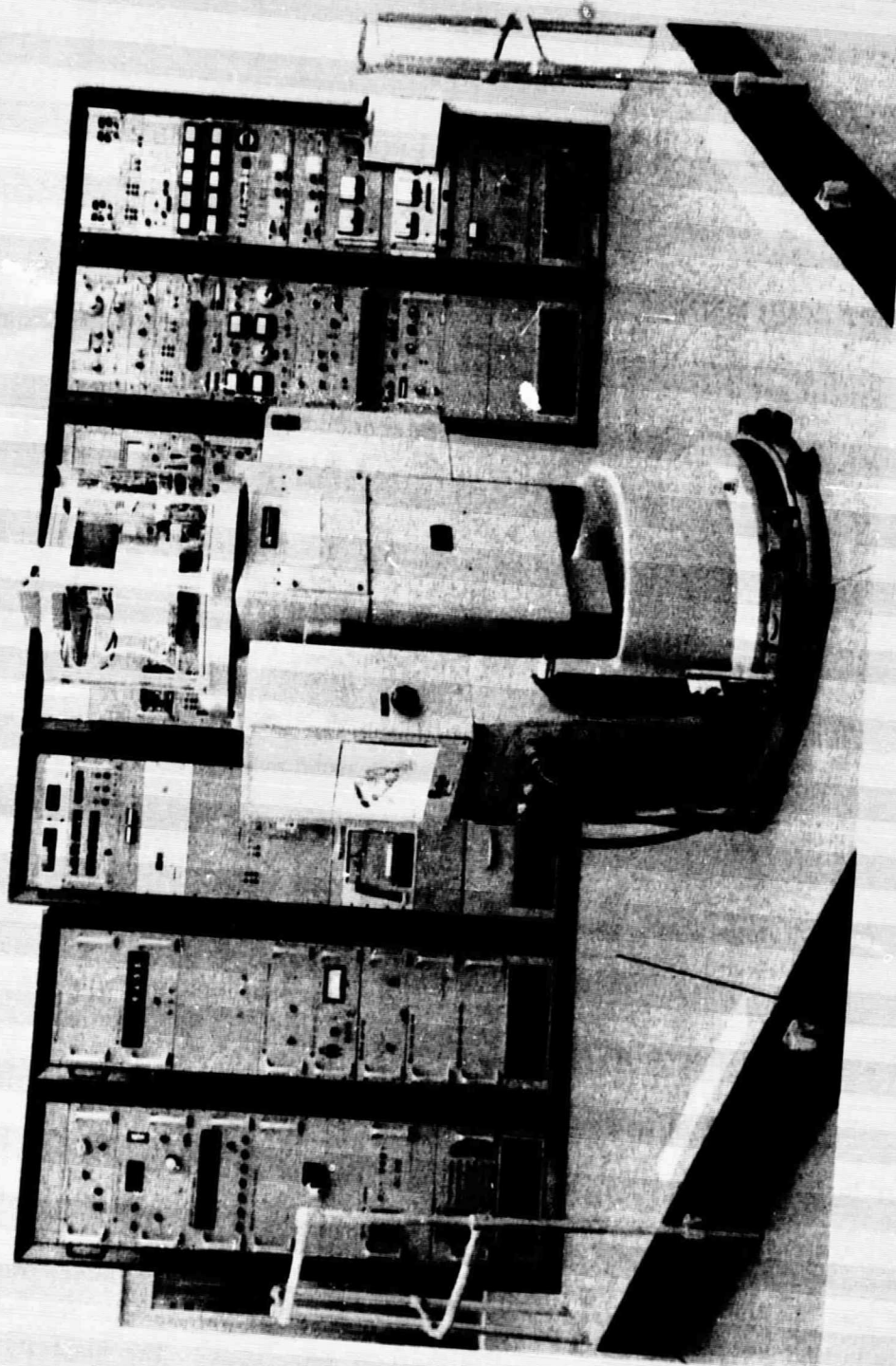


Figure 5-1. Test facility at The Charles Stark Draper Laboratory, Inc.

however, different sampling periods (10 to 3600 seconds) were used to investigate characteristics of the random noise.

The bias is defined by the following equation:

$$B = \frac{N}{\Delta t} SF_N$$

where:

- N = Net gyro output (pulses/sample)
- B = Instrument bias and earth rate component (gyro at fixed position, arc sec/s).
- $\Delta t$  = Sample time (seconds)
- $SF_N$  = Nominal SF (average SF for the range of input rate,  $\pm 100^\circ/s$ )

#### 5.2.1 Instrument Scale Factor

The test table is rotated uniformly with the RLG IA oriented vertically. The angle of rotation and elapsed time are accurately measured each time the net count of the RLG is printed. For this work one revolution's data was obtained while running the SF linearity test and ten revolutions' data were obtained while running the SF stability tests.

The angle of rotation divided by the net count plus or minus the bias and vertical component of earth rate, depending on the direction of table rotation, determines the calculated SF.

$$SF = \frac{R}{N \pm \frac{\Delta t(B + \omega_{IEV})}{SF_N}}$$

where:

- SF = Scale factor (arc sec/pulse)
- R = Angle of rotation (arc sec)
- $\omega_{IEV}$  = Vertical component of earth rate (arc sec/s).

After the instrument had completely settled (two days), the voltage or base plate mount temperature was changed to measure parameter sensitivities.



## SECTION 6

### TEST RESULTS

This report presents results on the following instrument performance characteristics:

#### Bias:

- Turn-on trends
- Stability and random drift
- Repeatability

#### Scale Factor:

- Turn-on trends and decay characteristics
- Stability
- Variation with input rate
- Repeatability
- Voltage and temperature sensitivities

The test results presented in this section were obtained from data taken between 5 March and 11 July 1975. Only one instrument was tested and, therefore, the results may not be representative of all instruments in this class.

With the base mount temperature at 90<sup>o</sup>F the laser and its electronics required 20 to 25 minutes to "warm-up" after turn-on before the output could be sampled to determine bias or SF. When the unit was ready for operation the READY light on the front panel would become lighted.

Unless otherwise stated, no known thermal gradients were introduced and the base plate was maintained at the recommended operating temperature of 90±1<sup>o</sup>F.

#### 6.1 BIAS TEST RESULTS

##### 6.1.1 Initial Transient

After warm-up the instrument exhibited an initial transient that required one-half hour to settle. Figure 6-1 is a typical bias plot and shows that the amplitude of bias across this interval was approximately 1<sup>o</sup>/h.

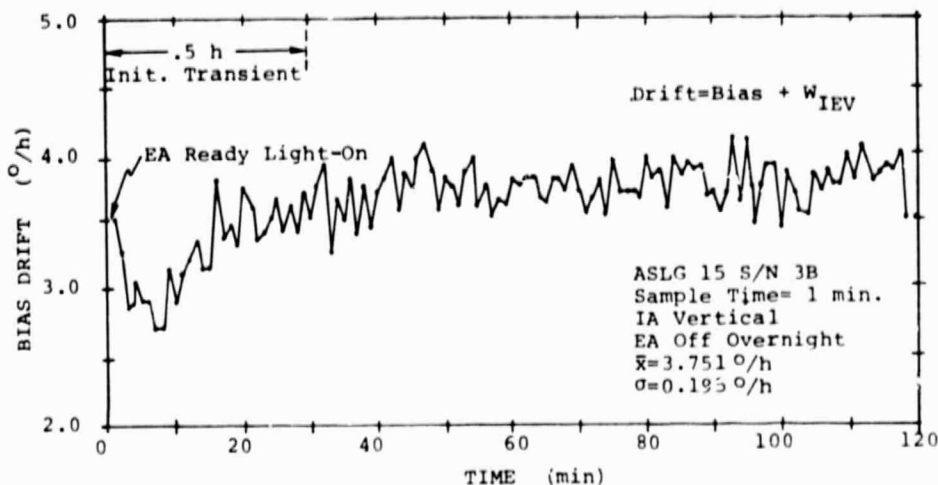


Figure 6-1. Bias stability (4-03-75).

#### 6.1.2 Bias Stability and Random drift

Figure 6-2 is a continuous 74 hour bias stability plot, obtained after the warm-up and initial transient. The sampling period was 600 seconds. This figure shows that there was no apparent change in the bias stability from start to finish.

Table 6-1 is a summary of all the bias stability tests from 5 March 1975 to 10 July 1975. The average magnitude of the bias plus vertical component of earth rate after the warm-up and transient was 3.8°/h (vertical component of earth rate was 10.1°/h). The peak-to-peak spread in magnitude of bias drift was 0.2°/h across turn-offs and cooldowns. Note that each test was started after the warm-up and transient.

Preliminary analysis of the one-sigma stability and random drift numbers shown in Table 6-1 indicated that the nature of bias data was not similar to the conventional rotating wheel gyros. In this instrument, the laser gyro, smaller sample times yielded correspondingly higher standard deviations as it exhibited a white noise characteristic. Additional testing and analysis to determine the exact nature of the laser's output are in progress. The results will be published in a subsequent report from NASA/Langley.

#### 6.1.3 Bias Repeatability

Figure 6-3 shows the bias drift repeatability for one and one half months across turn-offs and cooldowns. Each point plotted was the average of 100 second sample data for one hour after the warm-up and transient. The bias repeatability

ASLG 15 S/N 3B  
Sample Time= 600 s  
IA Vertical  
Test Started 4-11-75  
(After warm-up)

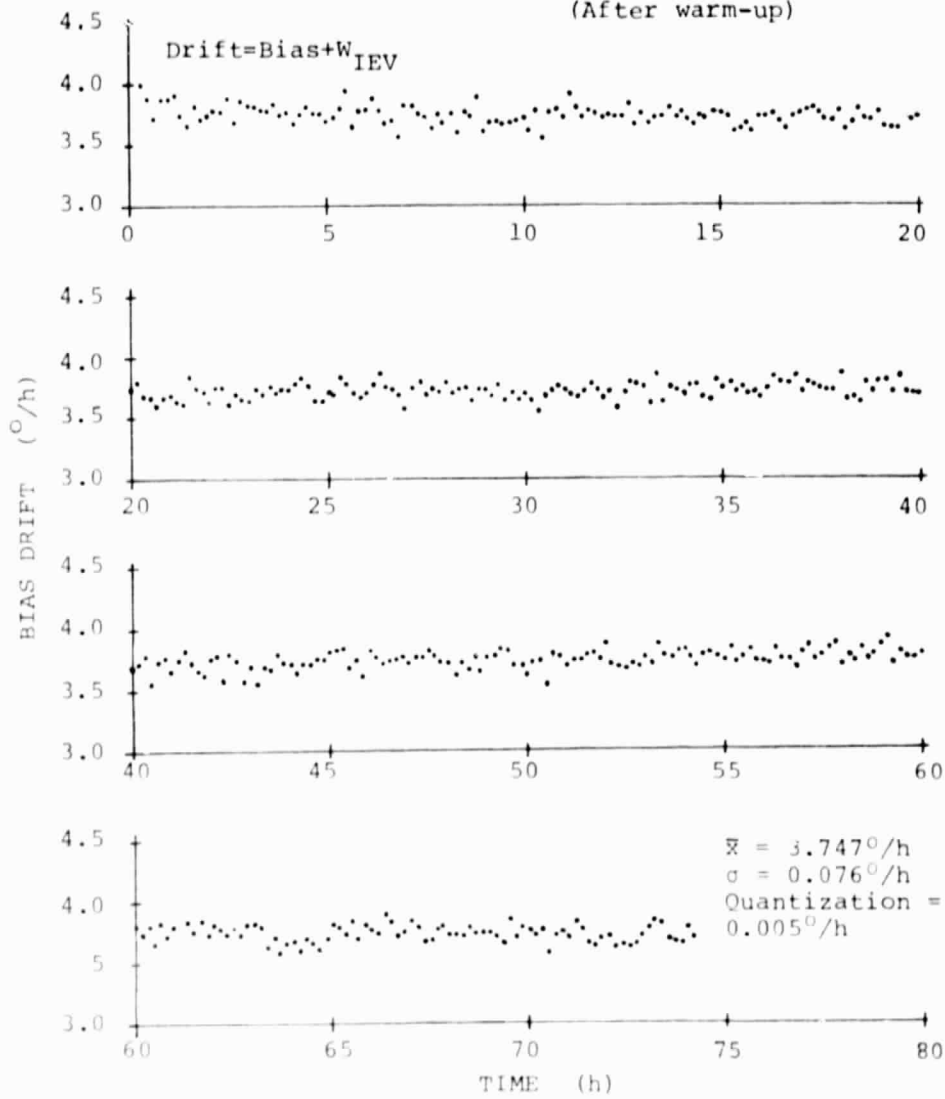


Figure 6-2. Bias stability (4-11-75).

Table 6-I. Bias stability and random drift

ASLG 15 S/N 3B  
IA Vertical

Date	Sample Time (s)	Test Duration (h)	Table Angle (deg)	EA Turn-On Time Before Test (h)	Drift Bias + $\omega_{IEV}$ ( $^{\circ}/h$ )	Stability (1 Sigma) ( $^{\circ}/h$ )	Randor Drift (1 Sigma) ( $^{\circ}/h/\sqrt{h}$ )
3- 5-75	10	.1	-	---	---	0.70	0.037
3- 5-75	10	.38	-	---	---	0.60	0.032
3- 6-75	60	9.07	-	6.5	---	0.232	0.030
3-11-75	60	2.08	-	1.25	---	0.280	0.036
3-17-75	60	3.76	-	3.0	---	0.228	0.029
3-31-75	600	40.2	0	144	3.694	0.065	0.026
4- 3-75	60	1.5	0	1.0	3.751	0.195	0.025
4- 3-75	600	30	0	2.5	3.668	0.067	0.027
4- 7-75	100	1.0	0	1.0	3.794	0.197	0.033
4-11-75	600	74	0	1.0	3.747	0.076	0.031
4-15-75	100	1.0	0	1.0	3.786	0.135	0.022
4-16-75	100	1.0	0	1.0	3.804	0.141	0.023
4-17-75	100	1.0	0	1.0	3.798	0.129	0.021
4-18-75	100	1.0	0	1.0	3.803	0.132	0.022
4-18-75	3600	77	0	1.0	3.749	0.034	0.034
4-23-75	100	1.0	0	1.0	3.731	0.193	0.033
4-24-75	100	1.0	0	1.0	3.747	0.196	0.033
4-25-75	100	1.0	0	1.0	3.797	0.146	0.024
4-28-75	100	1.0	0	1.0	3.876	0.185	0.031
4-29-75	100	1.0	0	1.0	3.796	0.185	0.031
5- 2-75	100	1.0	0	1.0	3.840	0.158	0.026
5- 5-75	100	1.0	0	1.0	3.874	0.142	0.024

Equipment on continuously.

(continued)

Table 6-1. Bias stability and random drift (cont.)

ASLG 15 S/N 3B  
IA Vertical

Date	Sample Time (s)	Test Duration (h)	Table Angle (deg)	EA Turn-On Time Before Test* (h)	Drift Bias + $\omega_{IEV}$ ( $^{\circ}/h$ )	Stability (1 Sigma) ( $^{\circ}/h$ )	Random Drift (1 Sigma) ( $^{\circ}/h/\sqrt{h}$ )
5- 6-75	100	1.0	0	1.0	3.805	0.156	0.026
5- 7-75	100	1.0	0	1.0	3.810	0.191	0.032
5- 8-75	100	1.0	0	1.0	3.894	0.172	0.029
5- 9-75	100	1.0	0	1.0	3.847	0.185	0.031
5-12-75	100	1.0	0	1.0	3.856	0.185	0.031
5-13-75	100	1.0	0	1.0	3.804	0.193	0.032
5-14-75	100	1.0	0	1.0	3.763	0.157	0.026
5-16-75	100	1.0	0	1.0	3.846	0.162	0.027
5-16-75	100	1.0	0	4.5	3.768	0.159	0.026
5-19-75	100	1.0	0	1.0	---	---	---
5-19-75	100	1.0	0	4.5	3.811	0.185	0.031
5-20-75	100	1.0	0	1.0	3.834	0.154	0.026
5-20-75	100	1.0	0	4.5	3.726	0.169	0.028
5-21-75	100	1.0	0	1.0	3.822	0.204	0.034
5-21-75	100	1.0	0	4.5	3.756	0.166	0.028
5-22-75	100	1.0	0	1.0	3.797	0.154	0.026
5-22-75	100	1.0	0	4.5	3.667	0.157	0.026
5-23-75	100	1.0	0	1.0	3.729	0.131	0.022
5-23-75	100	1.0	0	4.5	3.672	0.166	0.028
6-12-75	100	1.0	0	1.0	3.816	0.164	0.027
7- 2-75	100	1.0	0	8.0	3.710	0.170	0.028
7- 7-75	100	1.0	0	8.0	3.739	0.161	0.027
7- 8-75	100	1.0	0	8.0	3.684	0.164	0.027
7-10-75	100	1.0	0	8.0	3.666	0.164	0.027

\* Equipment on continuously.

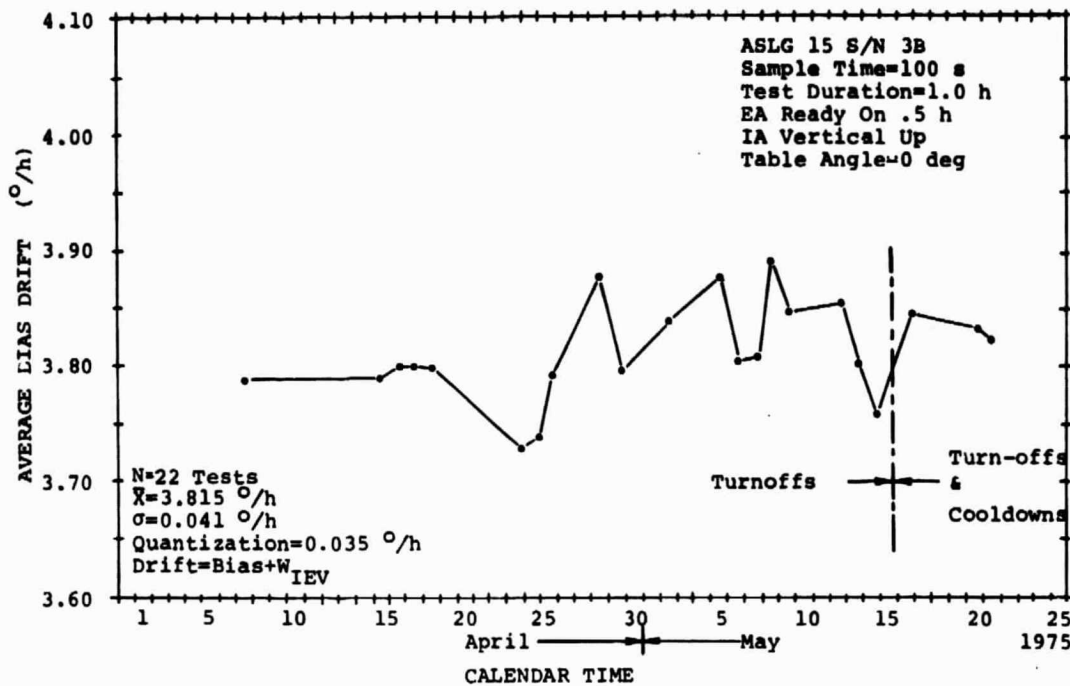


Figure 6-3. Drift repeatability across turn-offs and cooldowns.

among these tests was less than  $0.2$  °/h (peak-to-peak) and the one-sigma drift stability of the average value was  $0.04$  °/h. The Sperry "Installation, Operation and Performance Manual" that accompanied the instrument indicated that the one-sigma bias repeatability was  $0.2$  °/h. Interestingly, the one-sigma repeatability of the above tests was  $0.2$  °/h if the magnitude of bias is determined from one 100 second sample immediately after warm-up.

## 6.2 SCALE FACTOR TEST RESULTS

### 6.2.1 Initial Transient and Decay Characteristics

SF tests indicated that, after warm-up, the instrument had an initial one half hour transient period followed by an exponential decay with time constants greater than 4 hours. This section illustrates the characteristic transient and decay curves at several different input rates.

Figures 6-4 to 6-6 show the initial transient for one hour after warm-up for input rates of  $10$  °/s,  $30$  °/s and  $70$  °/s. The data for the first curve in each figure was obtained after an overnight turn-off. The subsequent curves had a

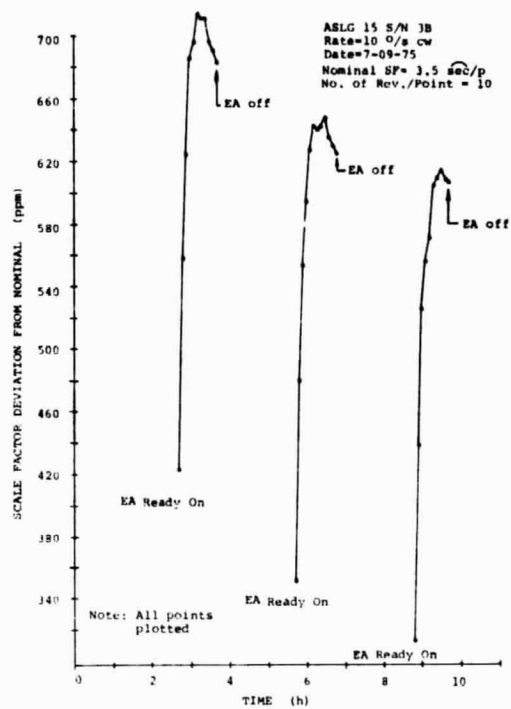


Figure 6-4. Scale factor: initial transient after warm-up (10<sup>0</sup>/s, cw).

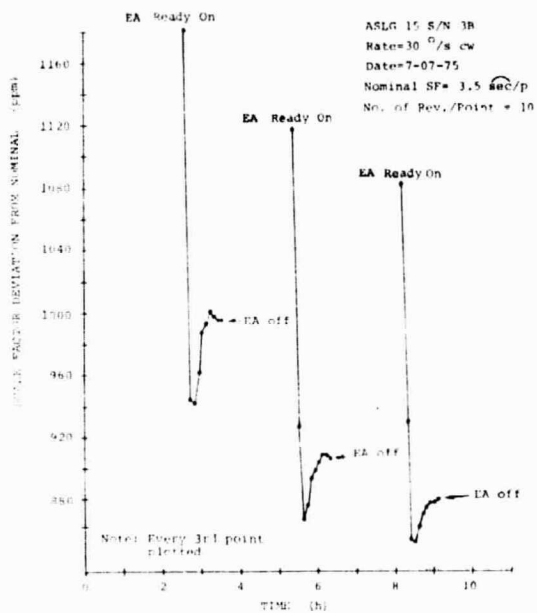


Figure 6-5. Scale factor: initial transient after warm-up (30<sup>0</sup>/s, cw).

REPRODUCIBILITY OF THE ORIGINAL PAGE IS POOR

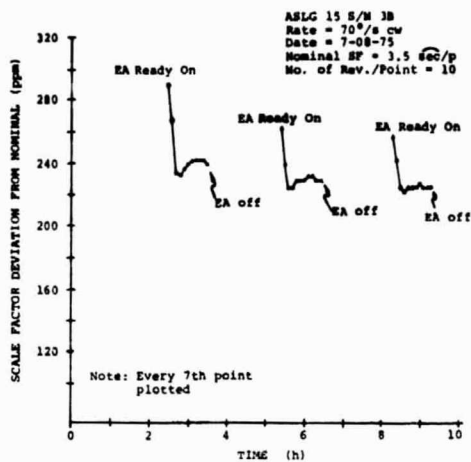


Figure 6-6. Scale factor: initial transient after warm-up (70°/s, cw).

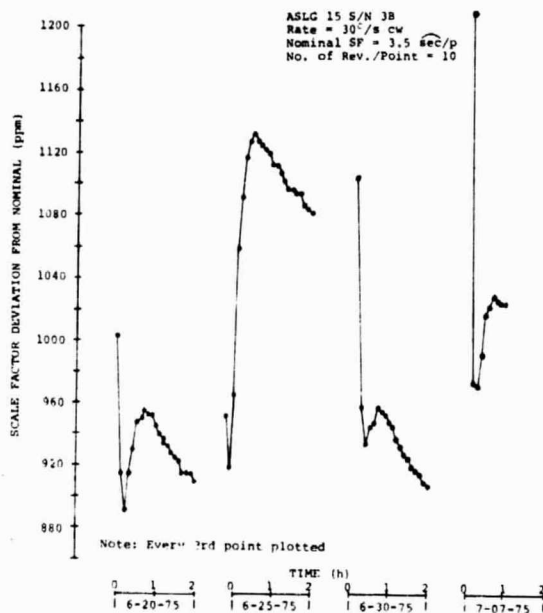


Figure 6-7. Scale factor: initial transient after warm-up (same rate from day to day).



one and one half hour turn-off. A comparison of these three figures show that:

- (1) The characteristic shape of the curves at each rate was consistent for data taken on the same day, however, this was not necessarily the case from day to day (see Fig. 6-7).
- (2) The starting point for all curves decreased in magnitude after the one and one half hour turn-off, probably due to an incomplete cooldown.
- (3) There was a definite decrease in the amplitude of the initial transient with increased input rate. At 10, 30 and 70<sup>o</sup>/s the initial transients were 280, 240 and 70 ppm, respectively.

Figure 6-8 shows the decay curves for 10, 20, 30, and 70<sup>o</sup>/s. The initial transients are not shown and the curves are superimposed with the initial points matched to illustrate the relative decay at different input rates. A comparison of these curves shows that there is a decrease in time constant and amplitude with increased input rate. However, like the initial transient curves, the decay curves are not repeatable from day to day. Figure 6-9 shows that the slope of the curve for the same rate changed with time.

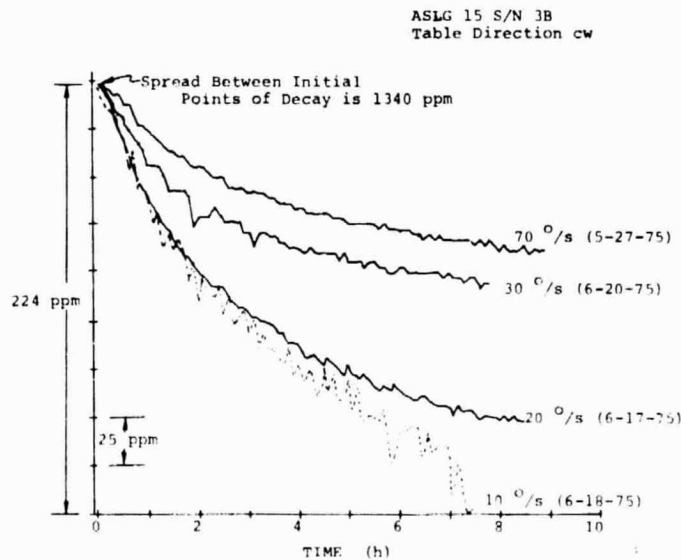


Figure 6-8. Scale factor decay after initial transient (four different rates).

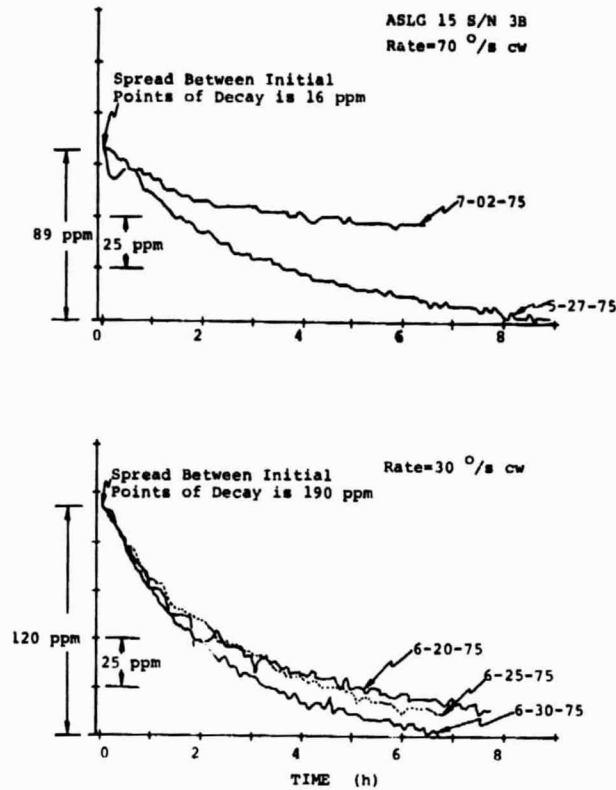


Figure 6-9. Scale factor decay after initial transient (same rate from day to day).

### 6.2.2 Scale Factor Stability

Figure 6-10 shows the first two and one half days of a SF stability test at a CW input rate of  $70^{\circ}/s$ . After one and one half days of testing the peak-to-peak stability of the following 24 hours was 8 ppm.

### 6.2.3 Scale Factor Variation with Input Rate

Figure 6-11 shows the spread in SF from  $5^{\circ}/s$  to  $100^{\circ}/s$  for both CW and CCW directions. Due to the lock-in phenomenon, the Sperry laser gyro is biased in two separate modes, a  $1/2$  Hz alternating bias when the magnitude of the input rate is less than  $12.5^{\circ}/s$  and a fixed bias when it is greater than  $12.5^{\circ}/s$ . This biasing technique is reflected in Fig. 6-11 with the discontinuity between  $10^{\circ}/s$  and  $15^{\circ}/s$ . The alternating bias region had a spread in SF of 114 ppm with an input rate from  $5^{\circ}/s$  to  $10^{\circ}/s$ . The fixed bias region had a spread in SF of 273 ppm with an input rate from  $15^{\circ}/s$  to  $100^{\circ}/s$ . The total spread in SF for the data shown in Fig. 6-11 was 320 ppm. The one-sigma SF linearity was 100 ppm.

REPRODUCIBILITY OF THE  
ORIGINAL PAGE IS POOR

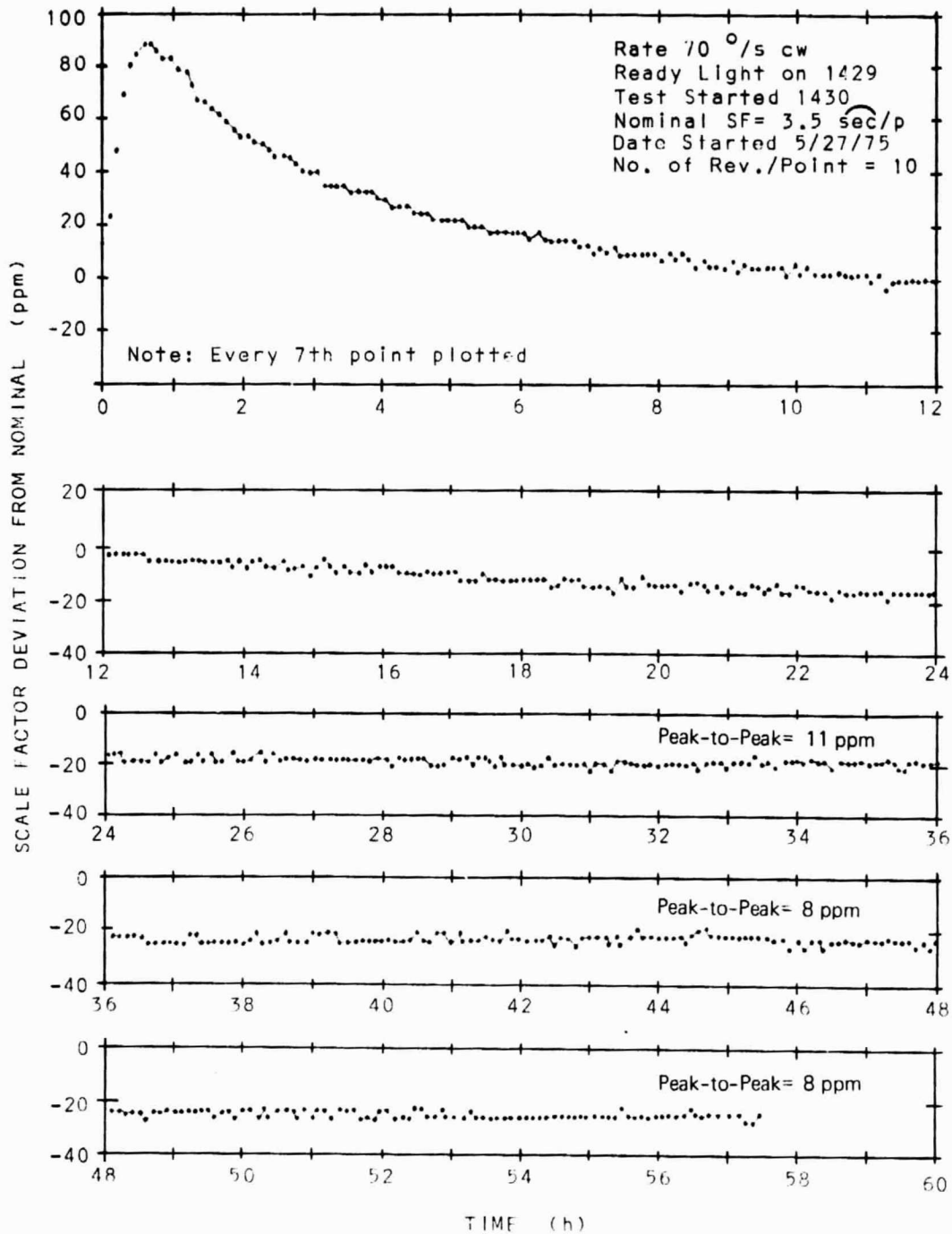


Figure 6-10. Long-term scale factor stability.

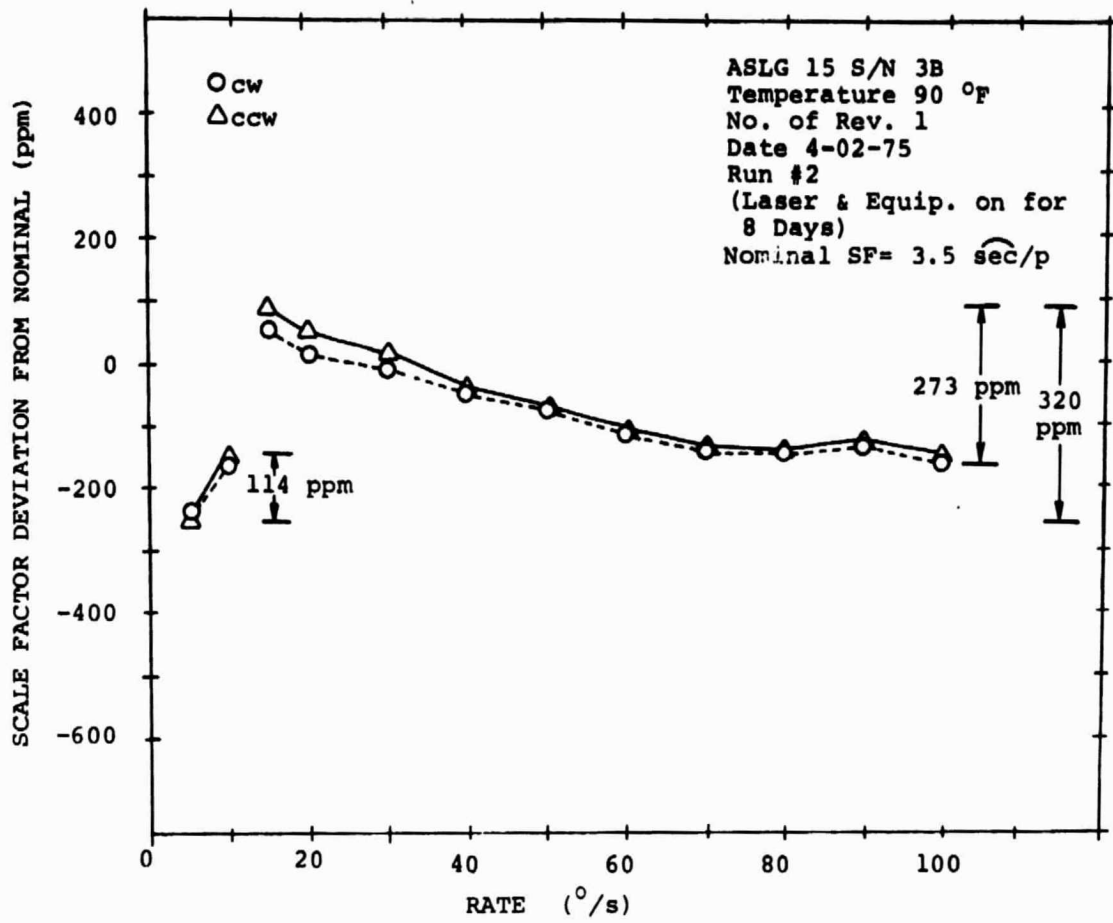


Figure 6-11. Scale factor variation with rate (5°/s to 100°/s).

The above SF linearity can be attributed, in part, to an uncertainty in the knowledge of the magnitude of fixed bias. A change in fixed bias with time would be reflected as a change in SF linearity with time. See Section 6.2.4, "Scale Factor Repeatability".

Figure 6-12 shows the spread in SF from 1°/s to 12°/s (alternating bias zone) for both CW and CCW directions. The spread in SF was 432 ppm. The one-sigma SF linearity was 90 ppm.

6.2.4 Scale Factor Repeatability

Figure 6-13 shows the SF drift with time across turn-offs and cooldowns for input rates of 10°/s, 20°/s, and 70°/s. Note that the peak-to-peak spread was 1370 ppm after a three month period.

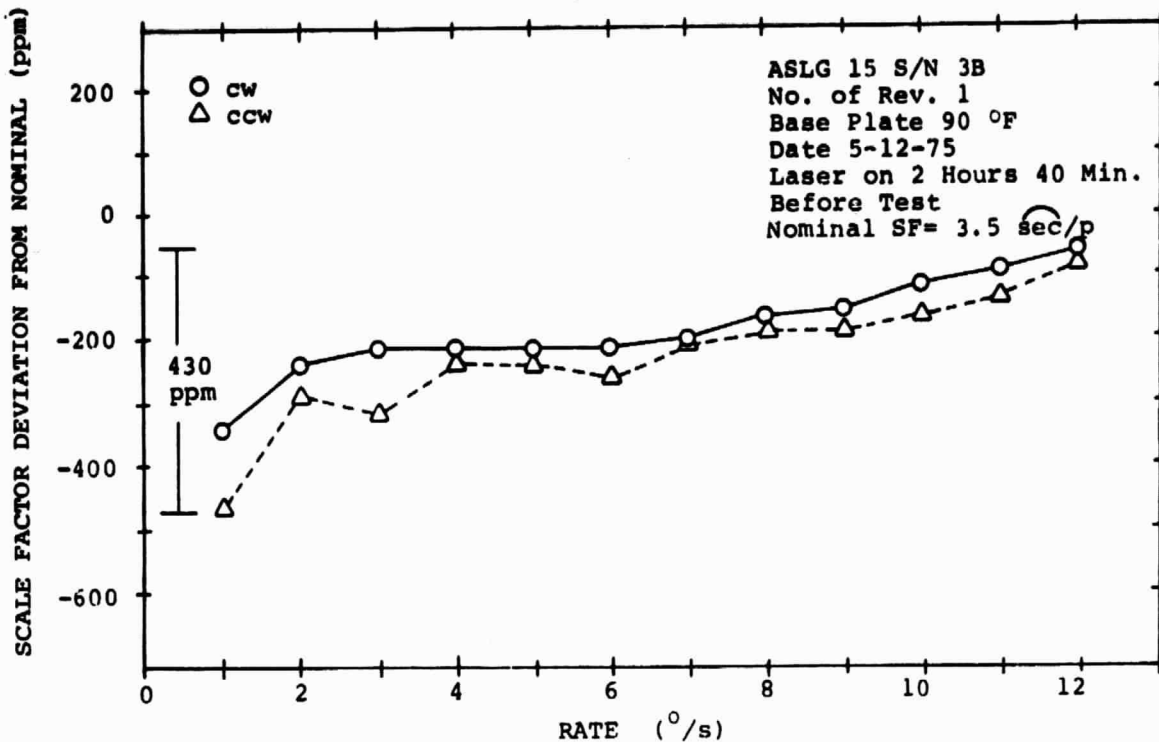


Figure 6-12. Scale factor variation with rate ( $1^{\circ}/s$  to  $12^{\circ}/s$ ).

The SF drift shown in Fig. 6-13 can be attributed to a drift in the fixed bias with time. The SF drift that occurred in the alternating bias zone ( $10^{\circ}/s$ ) should not show a drift with time. Any long-term bias change in the alternating bias zone would be cancelled with the alternating bias. However, in the fixed bias zone the long-term bias changes would be evidenced as a SF change with time. The same magnitude of bias change would have a greater effect on the lower input rates. The effects of the long-term bias change in the fixed bias zone is verified with the data shown in Fig. 6-13. The ratio of the input rates ( $20:70^{\circ}/s$ ) is approximately equal to the inverse ratio of their spread in SF ( $630:130$  ppm). Note that a change in fixed bias of approximately  $40^{\circ}/h$  would account for most of the SF drift.

In the CER-VIT SLG-15 instrument, Sperry presently compensates for the long-term bias drift by measuring the average magnitude of the positive and negative bias each time the instrument is turned on and by computationally maintaining this average magnitude.

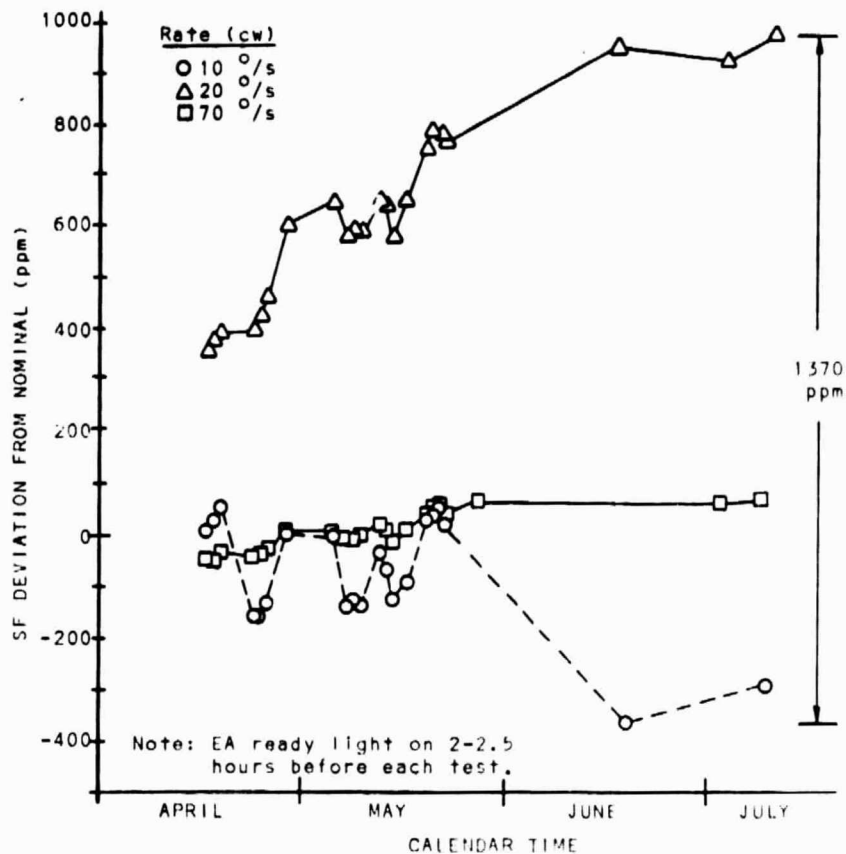


Figure 6-13. Scale factor vs. calendar time.

### 6.2.5 Voltage and Temperature Sensitivities

After establishing the initial transient, decay, and baseline stability, the voltage and base plate temperature were varied. The results were:

- (1) the SF is not sensitive (within measurement uncertainty) to supply voltage variations from 26 to 30 volts, and
- (2) the SF sensitivity to base plate temperature is approximately 3 ppm/°F from 88°F to 92°F.

## SECTION 7

### RECOMMENDATIONS

Since a system using this instrument will be flight tested by NASA/Langley, additional data should be obtained to model performance during system operation. Beyond those tests, it is recommended that any follow-on program should use a later model Sperry instrument suitable for production and address itself to the following additional types of tests:

- (1) Thermal tests at various ambients and gradients.
- (2) Performance during oscillations, particularly at the dither frequency.
- (3) Performance during vibration to investigate acceleration squared terms and structural resonance.
- (4) Centrifuge test to evaluate acceleration and acceleration squared terms.

While these tests are being run it is recommended that the laser gyro path length, discharge and magnetic mirror currents be monitored to obtain data correlations.